Electronic Supplementary Information

Nanostructured Cellulose Ionogels with Selective Anion Confinement for High-Efficiency Thermoelectric Harvesting

Legeng Li[a], Jiawang Zang[b], Bingjie Yang[a], Yongheng Cui[a], Ji Pan[b,*], Yingjie Zhou[a,*], Feng Yan[a,b,*]

[a] State Key Laboratory of Advanced Fiber Materials, College of Materials Science and Engineering, Donghua University, Shanghai 201620, China [b]Jiangsu Engineering Laboratory of Novel Functional Polymeric Materials, Department of Polymer Science and Engineering, College of Chemistry, Chemical, Engineering and Materials Science, Soochow University, Suzhou 215123, China

E-mail: zhouyj@dhu.edu.cn, fyan@suda.edu.cn

Experimental section

Materials

α-cellulose and allyl glycidyl ether (AGE) were supplied by Shanghai RHAWN Chemical Technology Co., Ltd. 1-ethyl-3-methylimidazolium dicyanamide ([EMIm][DCA], 98.0%) was provided by Monils Chemical Engineering Science and Technology (Shanghai) Co., Ltd. (3-Mercaptopropyl)trimethoxysilane (MTS) was purchased by Bide Pharmatech (Shanghai) Ltd. Urea (AR, 99.0%), Sodium hydroxide (98.0%) and 2,2-Dimethoxy-2-phenylacetophenone (99%), acetonitrile, methanol, and ether were supplied by Shanghai Titan Scientific Co., Ltd. Hydrochloric acid (HCl) and acetone were purchased from Shanghai Hushi Chemical Co.,Ltd. All chemicals were used as received.

Synthesis of the allyl cellulose (AC)

Cellulose was added to a 7 wt% NaOH/12 wt% urea aqueous solution and fully dissolved into a transparent 6 wt% cellulose solution through a cyclic freeze-thaw process. AGE was then added dropwise to the stirred cellulose solution until its molar ratio to the anhydroglucose units (AGU) of cellulose reached 9:1. The reaction was carried out at 30 ℃ under N_2 with continuous stirring for 24 hours. Subsequently, the mixture was thoroughly washed with ether and rotary evaporated at 30 °C to remove residual ether. The product was then precipitated from acetone and thoroughly washed with acetone to eliminate any remaining AGE. Next, the crude product was dissolved in deionized water and dialyzed for three days. Finally, the purified AC was obtained through vacuum freeze-drying for 48 hours.

Synthesis of POSS-8SH

5 mL MTS, 10 mL HCl, and 120 mL methanol were added to a 500 mL round-bottom flask. The reaction mixture was stirred under reflux at 90 °C for 24 hours. Subsequently, the white viscous precipitate was washed three times with methanol and then dissolved in 5 mL dichloromethane. This solution was then added dropwise into 100 mL of acetonitrile and recrystallized at -20 ℃ for 24 hours. Finally, the purified POSS-8SH was vacuum dried at 80 ℃ for 12 hours.

Preparation of the allyl cellulose/POSS-8SH click ionogel (APIG)

The allyl cellulose/POSS-8SH ionogel (APIG) was prepared via a thiol-ene click reaction. Typically, 0.3 g of allyl cellulose, certain masses (0 g, 0.09 g, 0.15 g, 0.21 g, 0.30 g) of POSS-8SH, and 0.03 g of DMPA were dissolved in 3 g DSMO under continuous stirring. The resulting transparent solution was cast into a polytetrafluoroethylene mold and photopolymerized under ultraviolet light for 30 minutes to form the organogel. The obtained organogel was subsequently immersed in acetone to exchange and remove the DMSO solvent. The solvent-exchanged gel was then immersed in a solution of [EMIm][DCA]/acetone for 3h. This immersion process was repeated 3 times to ensure complete ionic liquid infusion. Finally, the ionogels were dried at 80 °C for 2 hours to remove residual solvent. For nomenclature, the resulting materials are denoted as APIG-P_XI_Y, where X represents the weight percentage of POSS-8SH relative to allyl cellulose, and Y indicates the weight percentage of [EMIm][DCA] in the final ionogel.

Characterizations

Microscopic images of the APIG interior were acquired using a scanning electron microscope (Regulus 8230, Hitachi, Japan) and an atomic force microscope (Dimension FastScan/Icon, Bruker, Germany). The Fourier-transform infrared spectra (FT-IR) in the ATR mode were collected with a Perkin-Elmer FT-IR spectrometer (Spectrum 3, PerkinElmer, Germany). Raman spectra were collected by a Reflex Raman microspectrometer (inVia-Reflex, Renishaw, UK) at 532 nm. The transmittance data of the gel over the wavelength range of 400–800 nm were collected using a UV-Vis spectrophotometer (UV-1900i, Shimadzu, Japan). X-ray diffraction (XRD) patterns of the materials in the diffraction angle (2θ) range from 5 to 60° were recorded using X-ray diffractometer (D8 Advanced, Bruker, Germany). ^{1}H nuclear magnetic resonance (^{1}H NMR) spectra of the samples were recorded on Nuclear Magnetic Resonance Spectrometer (AVANCE400, Bruker, Germany). X-ray photoelectron scattering (XPS) (Escalab 250Xi, Thermo Fisher Scientific, USA) spectroscopy analysis was used to explore the elemental binding energy changes of ionogels. Small-angle X-ray scattering (SAXS) measurements were performed using a Xeuss 3.0 SAXS/WAXS system (Xeuss 3.0 XL, XENOCS, French) with Cu as radiation sources, the light tube power was 30 W and an X-ray with a wavelength of 1.54 Å was used as the radiation source with the beam area of 0.9 mm × 0.9 mm, and the sample-to-detector distances varied from 300 to 1700 mm. Mechanical properties are tested using a tensile pressure testing machine (UTM2103, Shenzhen Suns Technology Stock Co., Ltd., China). Two identical ionogel nanofiber membranes (one with a prefabricated notch) were mounted in pairs. The fracture energy (Γ) was determined by multiplying the integral area (ε) of the stress−strain curve of the notched specimen, where

the integral corresponds to the specimen's ultimate fracture strain, by the initial height (H). The specific calculation was performed using equation S1.

$$\Gamma = H \int_0^{\varepsilon_C} \sigma \, d\varepsilon \tag{S1}$$

Thermoelectric properties of APIG

The ionic conductivity (σ_i) of the ionogels were measured by electrochemical impedance spectroscopy (EIS) using an electrochemical workstation (Autolab PGSTAT302N, Switzerland) with a voltage amplitude of 100 mV in the frequency range of 1000 kHz-0.1 Hz. The ionogel was sandwiched between two stainless electrodes with an effect area of 1 cm^2, and the ionic conductivity was determined according to the equation (S2),[1]

$$\sigma_i = \frac{1}{RA}\frac{l}{} \tag{S2}$$

where R is the bulk resistance, l is the thickness of the ionogel, and A is the area of the ionogel.

The ionic Seebeck coefficient (S_i) was measured in a homemade temperature gradient planar configuration. Two commercial Peltier patches are used to generate temperature gradients, and the Ag wires with a diameter of 0.5 mm are used as electrodes. Two T-type thermocouples are employed to monitor the code and hot terminals of the ionogels. The generated thermal voltages were recorded on an electrochemical workstation (Autolab PGSTAT302N, Metrohm, Netherlands). Notably, a constant temperature and humidity chamber (HWS-150, China) was used to monitor the relative humidity (RH).

Thermal conductivities of all samples were measured by Hot Disk TPS 2500 S instrument (Hot Disk AB, Sweden) with a hot disk kapton sensor (5465 F1, radius 3.189 mm, the sample thickness range is no less than 2 mm) sandwiched between pairs of square

samples with the dimension of 30×30 mm^2. Three independent measurements were performed on each sample with a 15 min conditioning time between each measurement. Each sample was measured independently three times, and the average of the three-test data was taken.

The ionic power factors (PF_i) of ionogel can be calculated by the Equation (S3)[2]

$$PF_i = S_i^2 \sigma_i \tag{S3}$$

The ZT_i value can be calculated by the Equation (S4)[3]

$$ZT_i = \frac{S_i^2 \sigma_i T}{\kappa} \tag{S4}$$

where S_i is the ionic Seebeck coefficient, σ_i is the ionic conductivity, κ is the thermal conductivity, and T is the absolute temperature.

Simulations

Ionogel modeling

The Amorphous Cell module was employed for APIG-P_0I_{60} (POSS-free, System I) and APIG-P_5I_{60} (POSS-containing, System II) models. The incorporation number of anhydroglucose and [EMIm][DCA] unit (AGU) molecules into the cell is 120 and 380 for System I, and 120 and 360 for System II. The quantity of crosslinking agent required is determined by experimental protocols. Molecular dynamics (MD) simulations were performed using the LAMMPS software package.

MD simulations on thermal conductivity of ionogels

The OPLS all-atom force field was adopted (bond angle: harmonic; dihedral angle: OPLS; Van der Waals: LJ/cutoff 12.0 Å). Non-equilibrium molecular dynamics (NEMD)

simulations were conducted, with heat flux applied via the fix ehex command (+0.05 eV ps^{-1} for hot end; -0.05 eV ps^{-1} for cold end). Temperature gradients were statistically analyzed by compute chunk/atom with a bin width of 1.0 Å, sampled every 1000 steps. The steady-state gradient was the average of 28,000–34,000 steps, with error bars representing standard deviation (1σ). For data processing, z-direction temperature distributions were extracted from LAMMPS output files; linear fitting was performed on temperature profiles, with the slope being ∇T; thermal conductivity κ was calculated using Fourier's law $\kappa = -J_q/\nabla T$ in combination with input heat flux J_q.

MD simulations on ion migration of ionogels

An all-atom force field was employed, and energy minimization was conducted as a preliminary step. Subsequently, NPT ensemble equilibration was carried out at 300 K for 0.5 ns, followed by NVT ensemble equilibration for another 0.5 ns, and a final equilibration of 1 ns. All simulations in this work adopted a time step of 1 fs and a pressure parameter of 1 atm. Temperature and pressure were regulated via a Nose-Hoover thermostat (damping parameter: 0.2 ps) and a barostat (damping parameter: 1 ps), respectively. Subsequent data analysis was performed using 1 ns of production run trajectories, calculated via the Python-based MD analysis code. The specific calculation methods are as follows:

Ionic conductivity calculation

The ionic conductivity of the APIG can be calculated by Equation (S5) (Nernst–Einstein Approximation)[4]

$$\sigma_{NE} = \frac{e^2}{Vk_BT}\left(N_+ Z_+^2 D_+ + N_- Z_-^2 D_-\right) \quad \text{(S5)}$$

where e represents the elementary charge, V is the volume of the system, k_B denotes the Boltzmann constant while T signifies the temperature of the system. The charges on the cation and anion are given by Z_+ and Z_-, while the respective self-diffusion coefficients are labeled as D_+ and D_-; N_+ and N_- indicate the number of cations and anions, respectively.

Mean square displacement (MSD) calculation

The MSD of ions can be calculated by the Equation (S6) (Einstein relation method)[5]

$$MSD(t) = \frac{1}{N}\sum_{i=1}^{N}\left[r_i(t) - r_i(0)\right]^2 \quad \text{(S6)}$$

where $r_i(t)$ is the displacement of the particle at time t, $r_i(0)$ is the displacement of the particle at the initial time, and N is the number of particles.

Diffusion coefficient calculation

Based on the linear relationship between MSD and time, the diffusion coefficient was calculated via the Einstein equation (S7)[6]

$$D = \lim_{t\to\infty}\left[r_i(t) - r_i(0)\right]^2/2d_i t \quad \text{(S7)}$$

where d_i is the dimension of space, t is the simulation time and $[r_i(t)\text{-}r_i(0)]^2$ is the mean square displacement (MSD).

Entropy change calculation

Based on the simulated entropy value and thermodynamic relationship, calculate the entropy change parameter α using equation

$$\alpha = dS/dT \tag{S8}$$

where S is the simulated entropy value and T is the system temperature. The slope obtained by calculating the derivative (dS/dT) of entropy (S) with respect to temperature (T) through linear regression is the entropy change. This parameter characterizes the contribution of entropy change during ion migration process.

Supplementary results

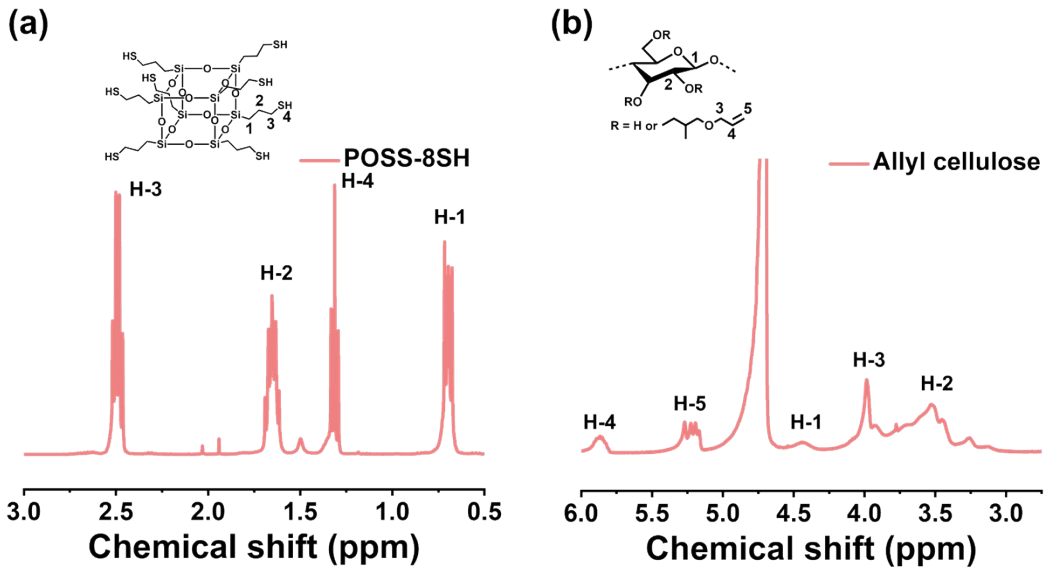

Figure S1. ^{1}H NMR spectra of a) POSS-8SH and b) allyl cellulose (AC). The presence of ^{1}H NMR peaks corresponding to the hydrogen atoms on the side chains of POSS-8SH and those attached to the C=C double bonds of AC confirms the successful synthesis of these two materials.

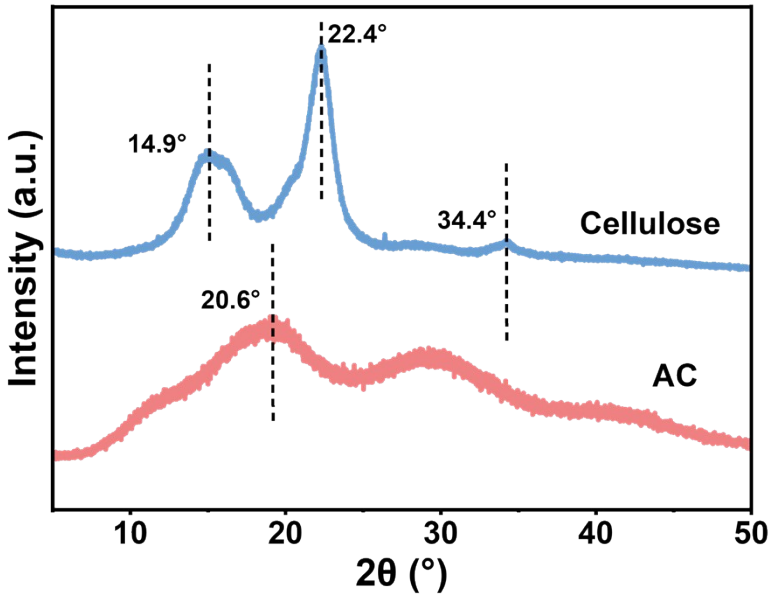

Figure S2. X-ray diffraction (XRD) patterns of cellulose and AC. The significant reduction in crystallinity for AC suggests the successful conversion of cellulose I to cellulose II upon the chemical modification by NaOH/urea.

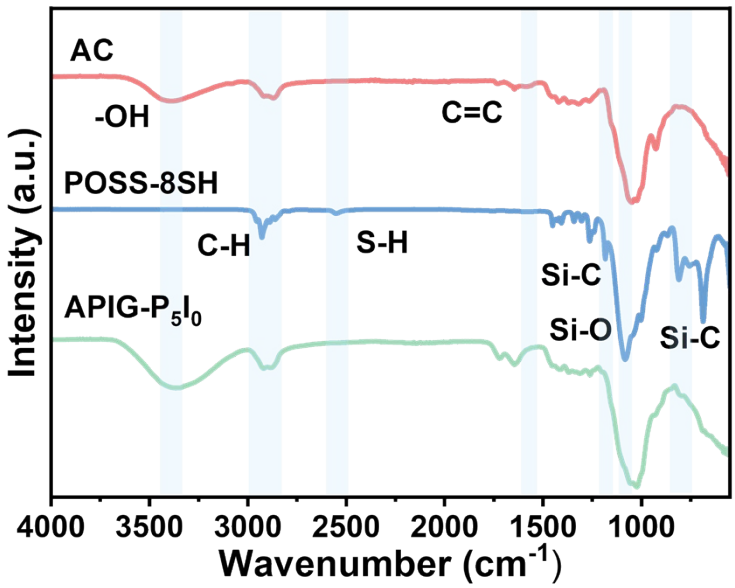

Figure S3. FT-IR spectra of AC, POSS-8SH and APIG-P_5I_0. Compared with the FTIR spectra of AC and POSS-8SH, the characteristic C=C stretching vibration peak (1570 cm^{-1}) and -SH stretching vibration peak (2250 cm^{-1}) disappeared for APIG-P_5I_0, suggesting that the thiol-ene click reaction between AC and POSS-8SH was successfully accomplished.

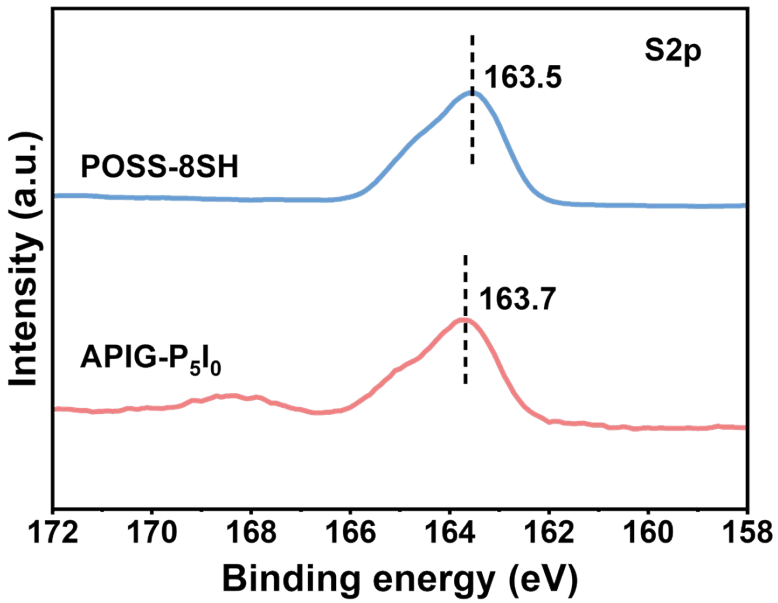

Figure S4. High-resolution XPS spectra of S2p for POSS-8SH and APIG-P_5I_0. The binding energy of S 2*p* shifted from 163.5 eV in POSS-8SH to 163.7 eV in APIG-P_5I_0, confirming the formation of C-S bonds.

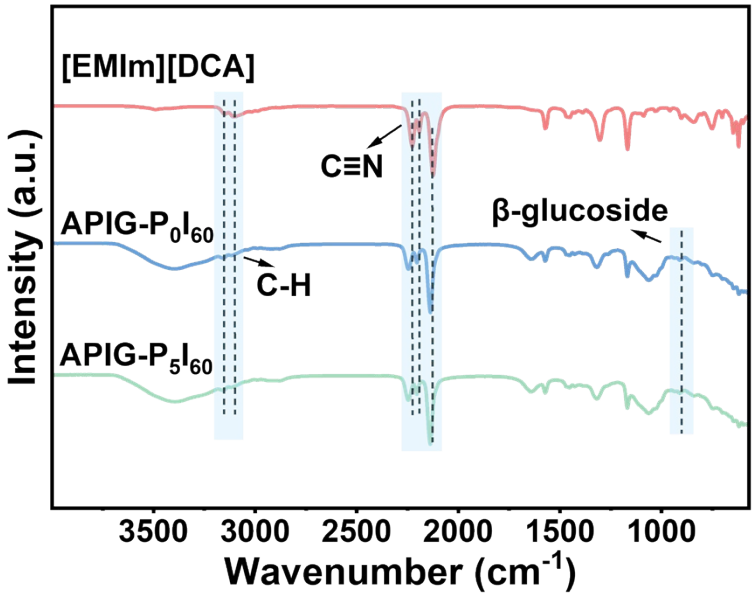

Figure S5. FT-IR spectra of [EMIm][DCA], APIG-P_0I_{60} and APIG-P_5I_{60}. Compared with the POSS-free counterpart, the stretching vibrations of C2-H (3116 cm^{-1}) and C4,5-H (3158 cm^{-1}) in $EMIm^+$ within APIG-P_5I_{60} undergo a red shift, shifting to 3114 cm^{-1} and 3156 cm^{-1}, respectively. In contrast, the -C≡N stretching vibration in APIG-P_5I_{60} exhibits a blue shift, moving from 2136 cm^{-1} to 2137 cm^{-1}. These opposite shifts indicate that the polymer matrix facilitates the dissociation of the cations and the anions.

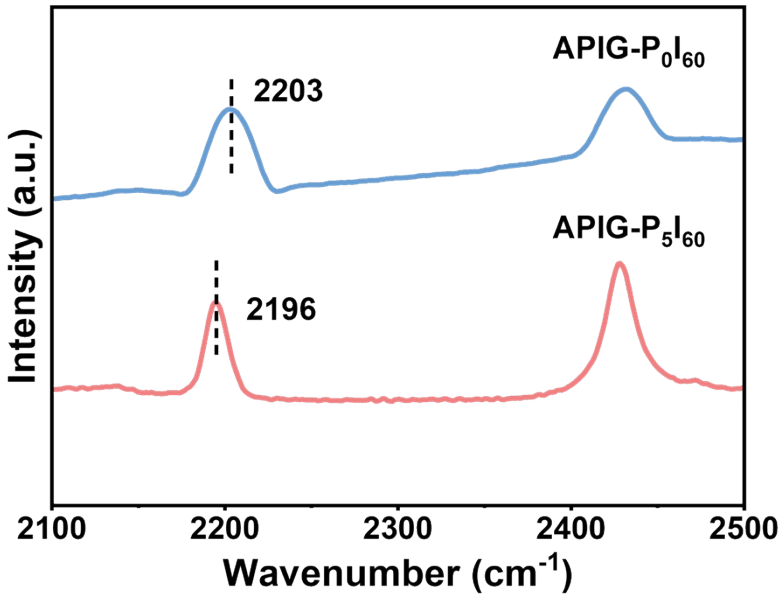

Figure S6. Raman spectra of APIG-P_0I_{60} and APIG-P_5I_{60}. The -C≡N stretching vibration shifts from 2203 cm^{-1} to 2196 cm^{-1} upon the POSS incorporation, indicative of a coordination interaction between the Si atoms in POSS cage and the N atoms of the -C≡N group in the anions.

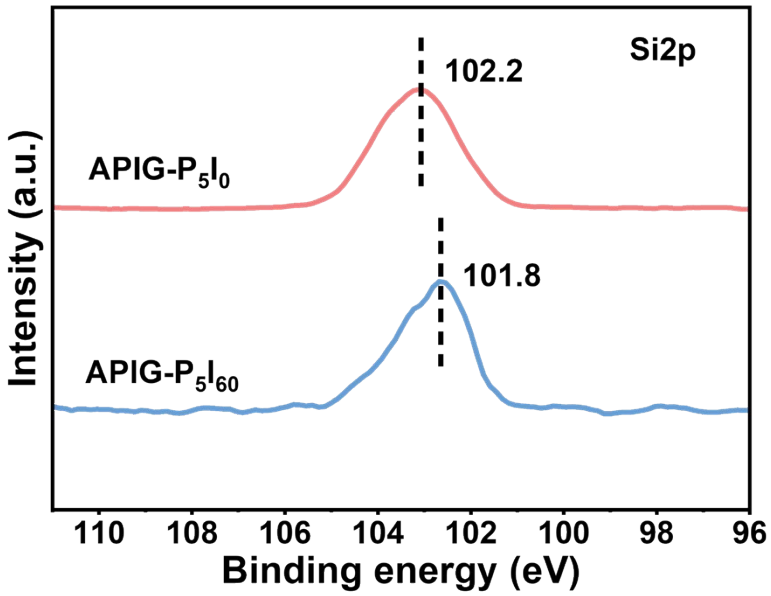

Figure S7. High-resolution XPS spectra of Si *2p* for APIG-P_5I_0 and APIG-P_5I_{60}. The binding energy of Si *2p* increases from 101.8 eV to 102.2 eV after [EMIm][DCA] infusion, indicating a decrease in electron density on the POSS cage due to dipole-dipole interactions with the anions.

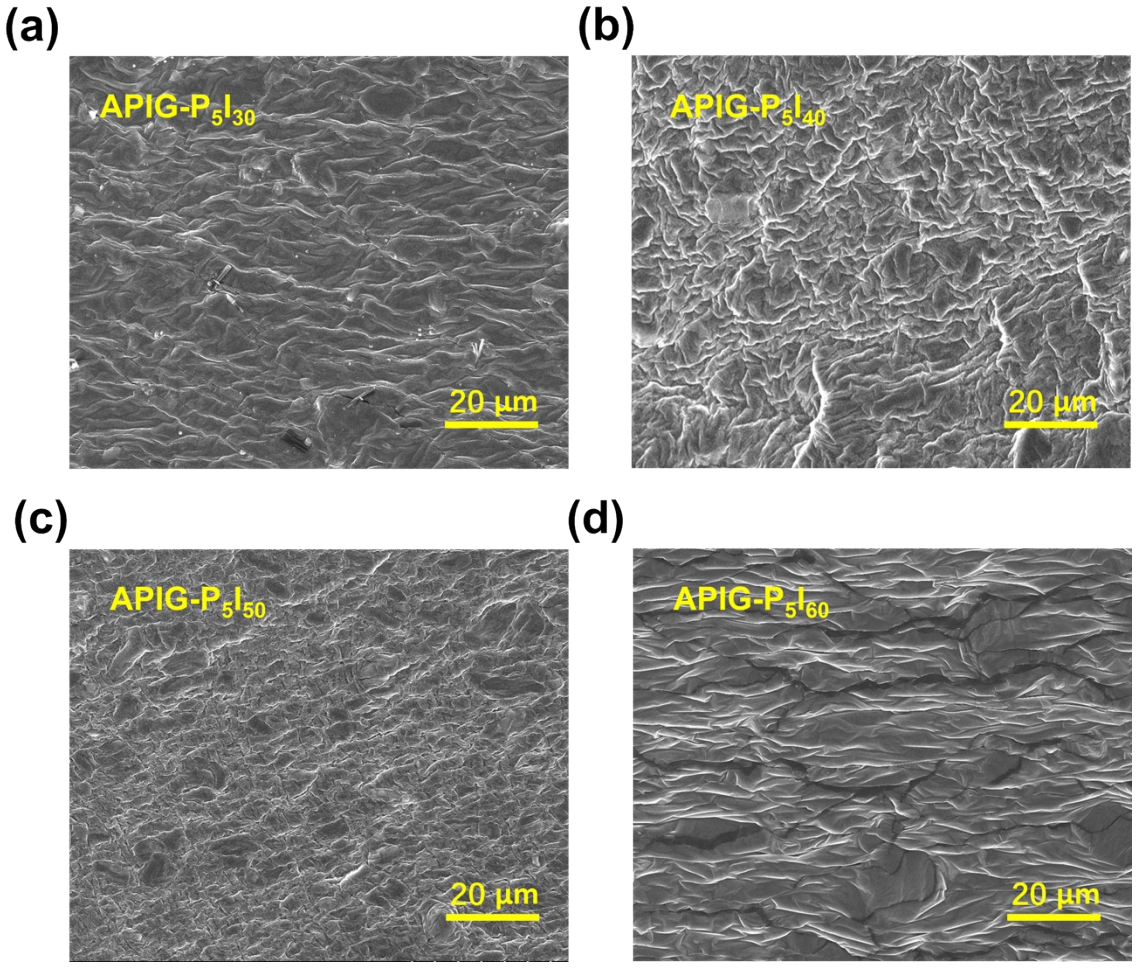

Figure S8. SEM images of a) APIG-P_5I_{30}, b) APIG-P_5I_{40}, c) APIG-P_5I_{50} and d) APIG-P_5I_{60}.

As the concentration of [EMIm][DCA] increases, the microphase separation of the ionogels becomes more significant.

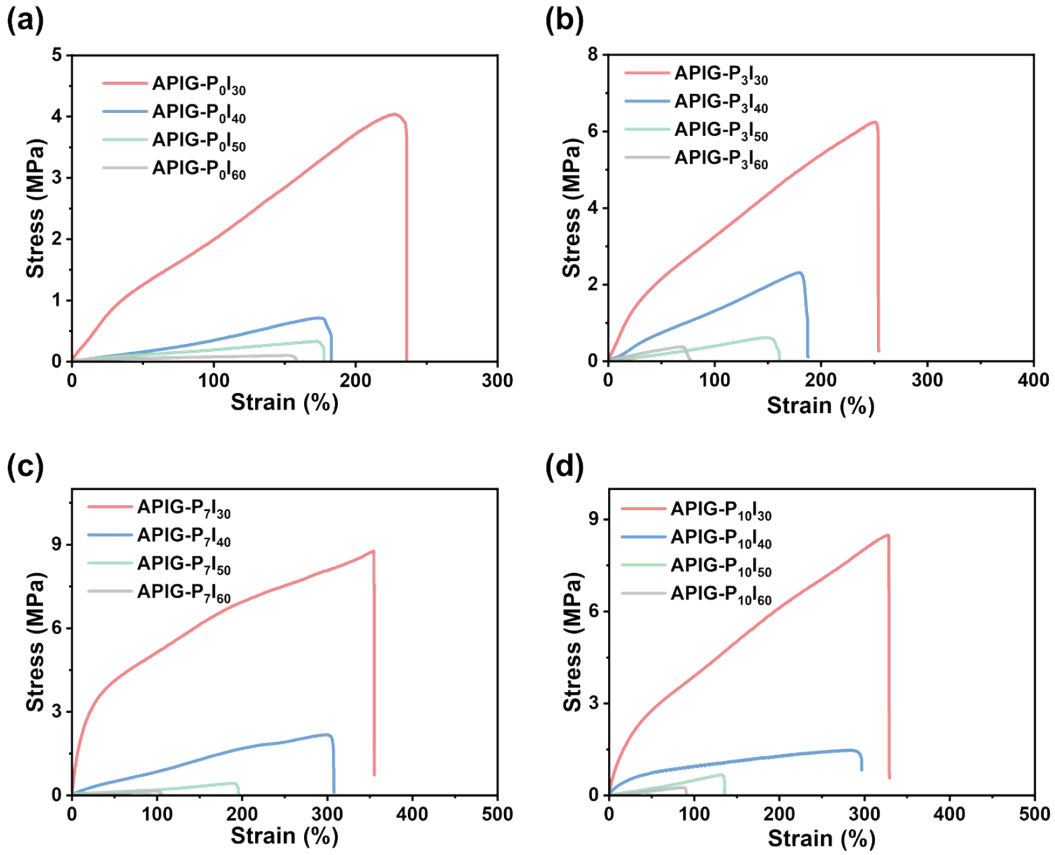

Figure S9. Tensile stress–strain curves of the a) APIG-$P_0I_{30\text{-}60}$, b) APIG-$P_3I_{30\text{-}60}$ and c) APIG-$P_7I_{30\text{-}60}$ and d) APIG-$P_{10}I_{30\text{-}60}$. As the content of [EMIm][DCA] increases from 30% to 60%, a significant decrease in tensile strength and Young's modulus was observed.

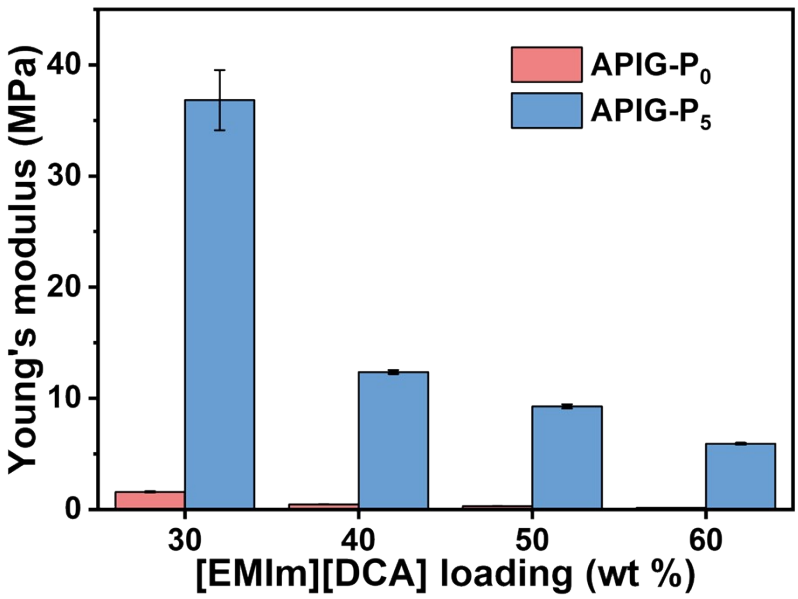

Figure S10. Young's modulus of the APIG-P_0I_{30-60} and APIG-P_5I_{30-60}.

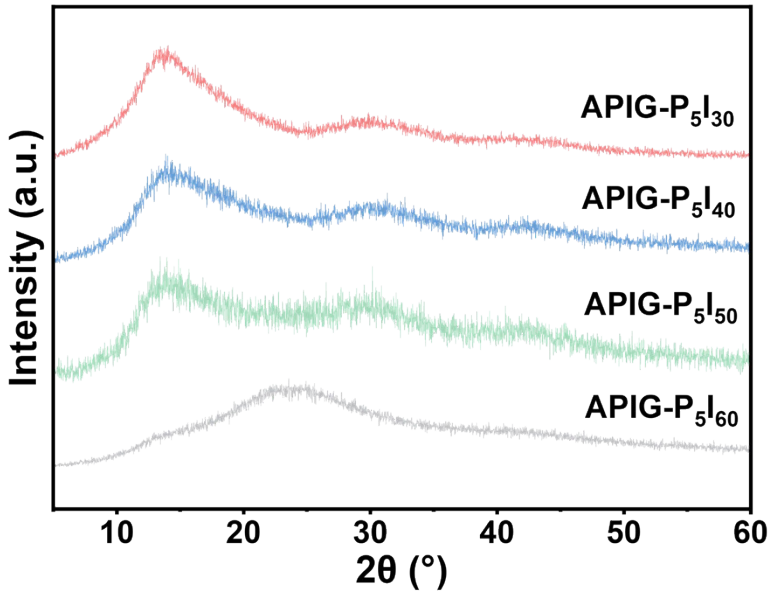

Figure S11. X-ray diffraction patterns of APIG-P_5I_{30}, APIG-P_5I_{40}, APIG-P_5I_{50} and APIG-P_5I_{60}. The crystallinity of APIG-P_5 exhibits a decreasing tendency with increasing [EMIm][DCA] concentration.

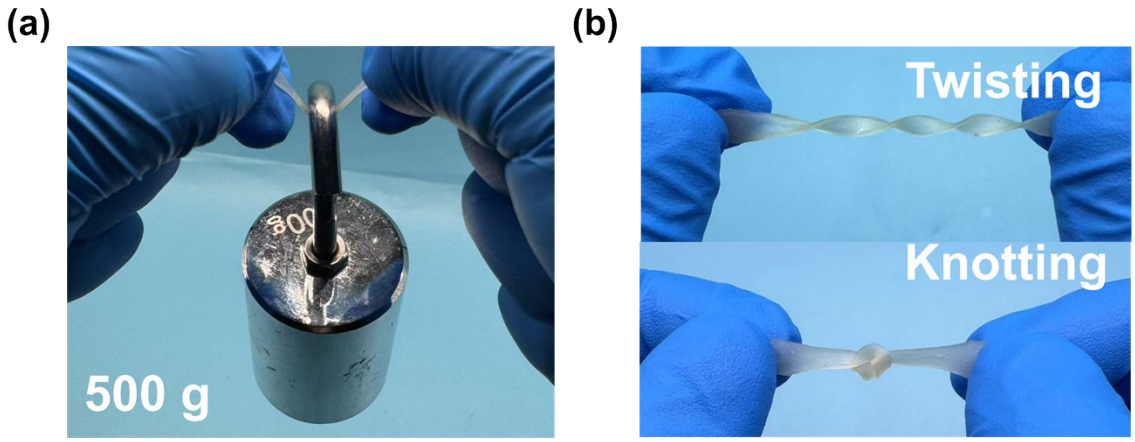

Figure S12. a) Digital photos of the APIG-P_5I_{30} (0.062 g, 4×0.3×0.06 cm^3) holding 8000 times its own weight. b) Twisting and knotting form of APIG-P_5I_{30} under external forces.

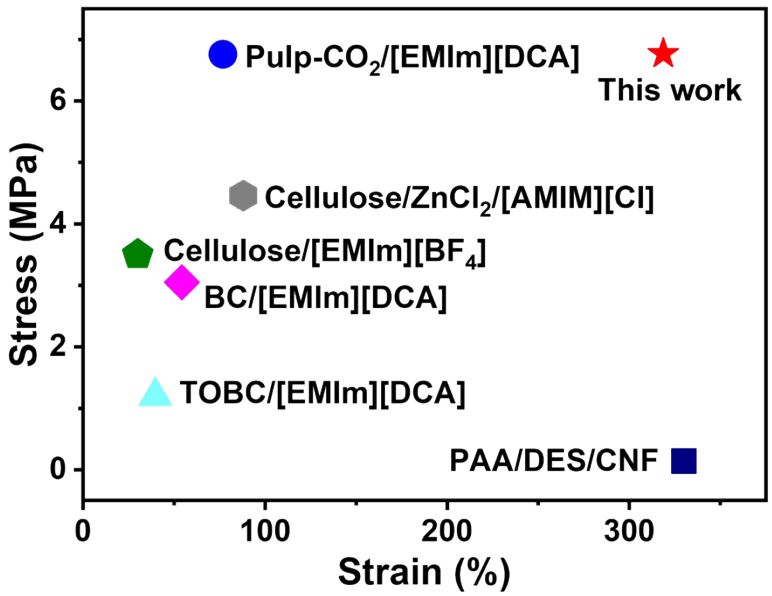

Figure S13. Comparison of mechanical properties of APIG-P_5I_{30} with reported cellulose-based ionogel.

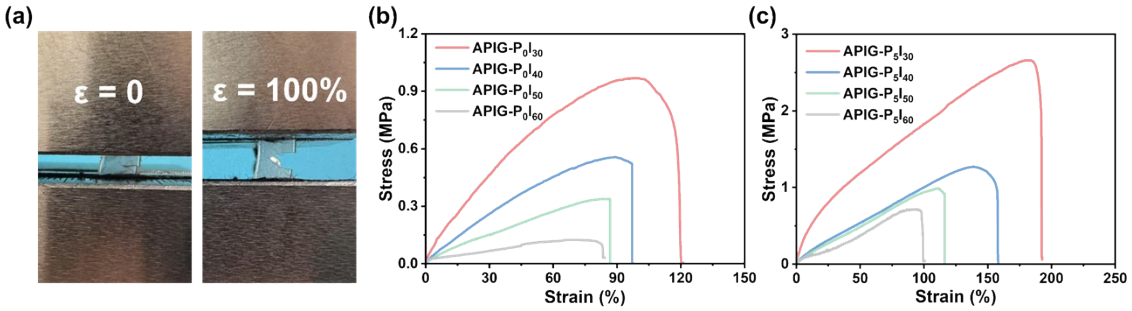

.

Figure S14. a) Photographs of notched APIG-P_5I_{60} (stretched to 100 %). b-c) Crack propagation stress-strain curves of b) APIG-P_0 and c) APIG-P_5.

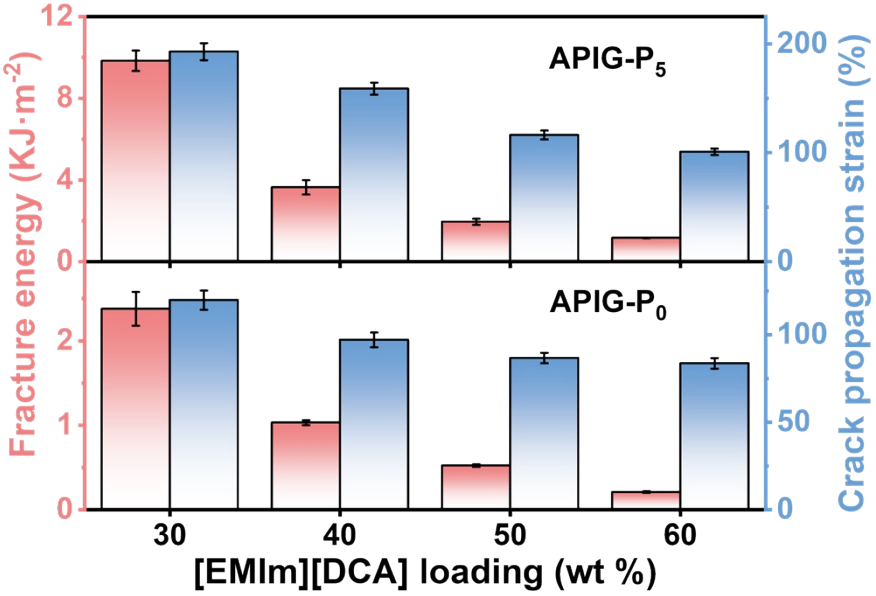

Figure S15. Crack propagation strain and corresponding fracture energy of the APIG-P_0 and APIG-P_5. The crack propagation strain and corresponding fracture energy of APIG-P_5 have been significantly improved upon incorporation with the POSS-8SH.

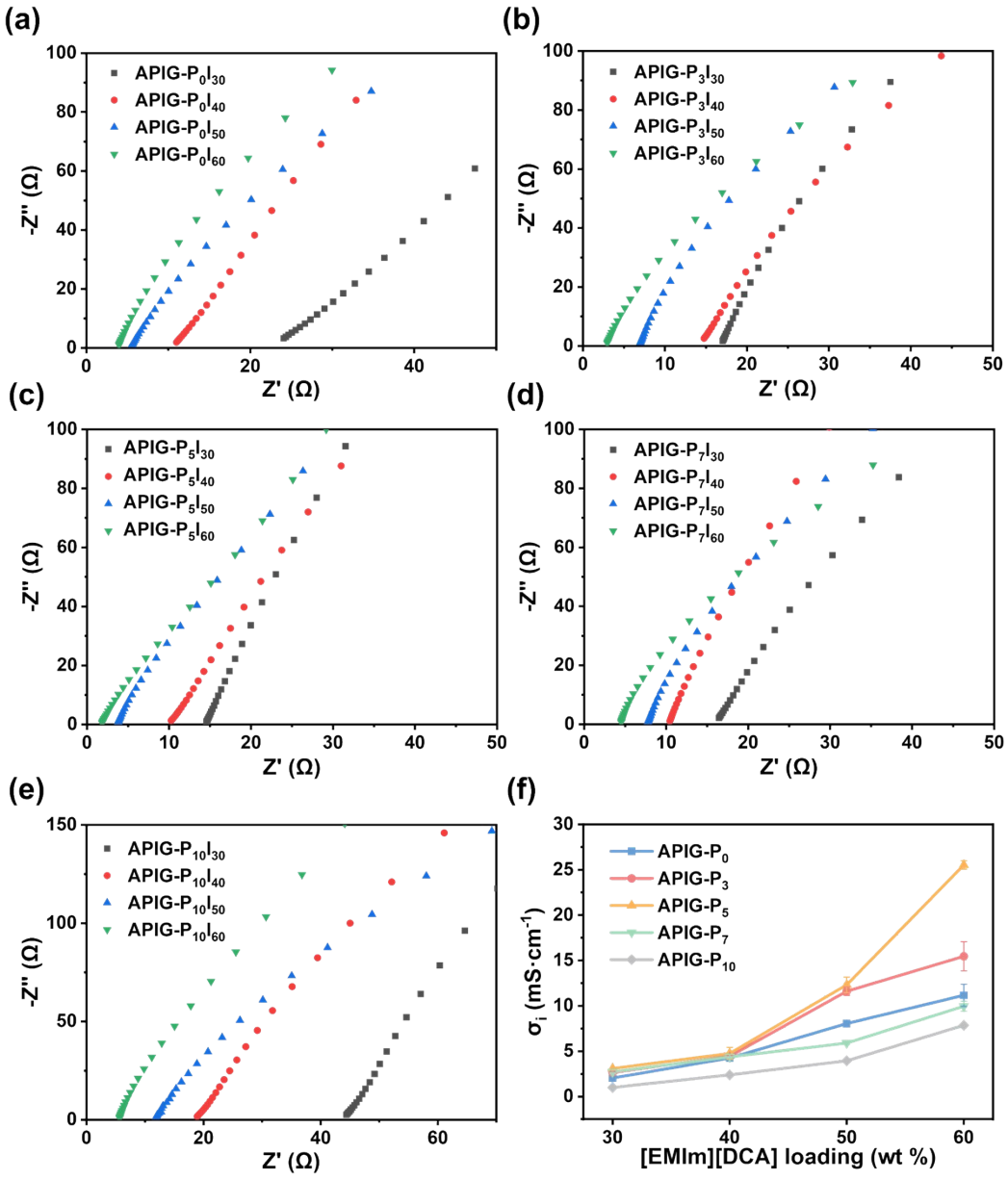

Figure S16. Nyquist plots of a) APIG-P_0, b) APIG-P_3, c) APIG-P_5, d) APIG-P_7 and e)

APIG-P_{10}. f) Ionic conductivity of APIG with various POSS-8SH concentration and [EMIm][DCA] loading.

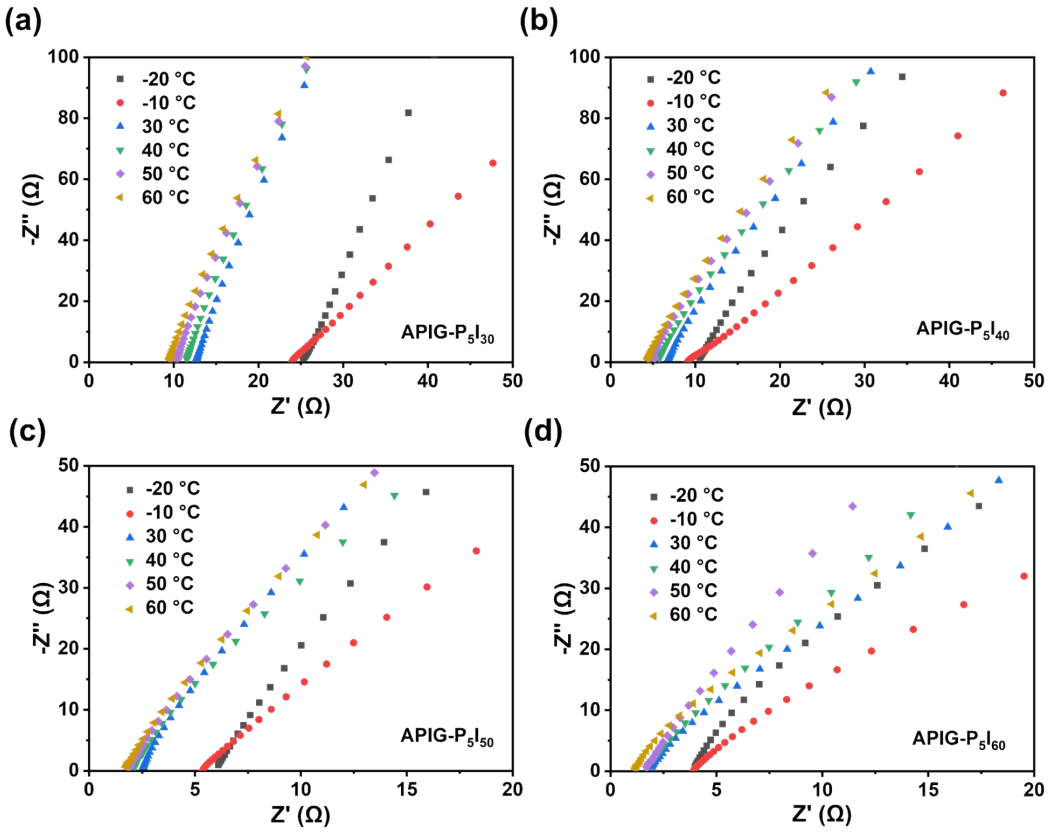

Figure S17. Nyquist plots of a) APIG-P_5I_{30}, b) APIG-P_5I_{40}, c) APIG-P_5I_{50}, d) APIG-P_5I_{60} at different temperatures.

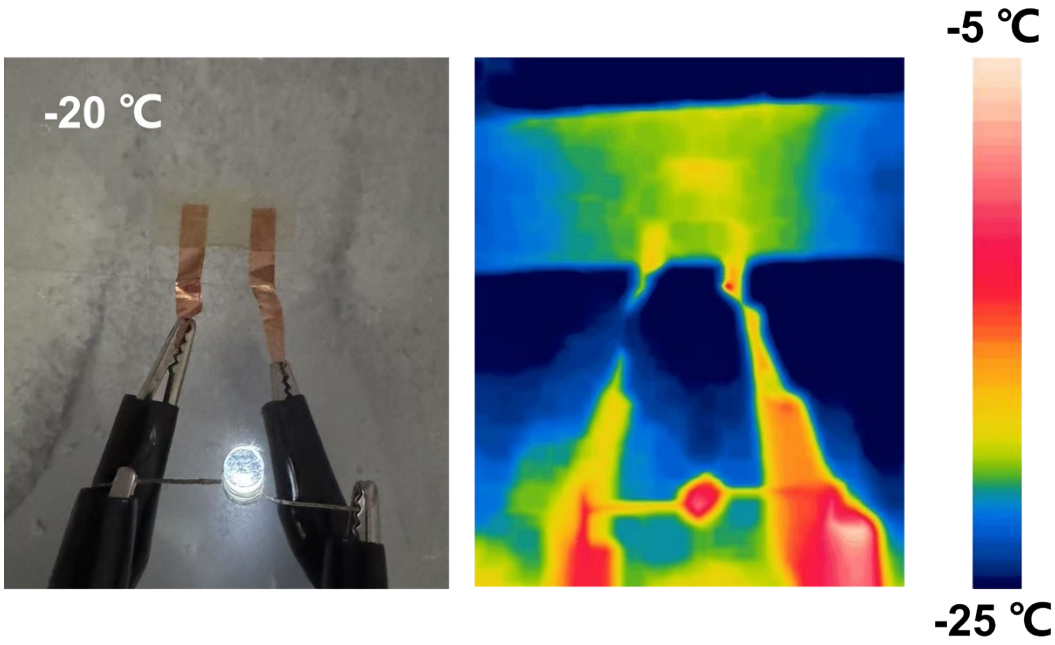

Figure S18. Digital photos and infrared photos of using APIG-P_5I_{60} as a conductor to light up LED in low temperature (-20 ℃).

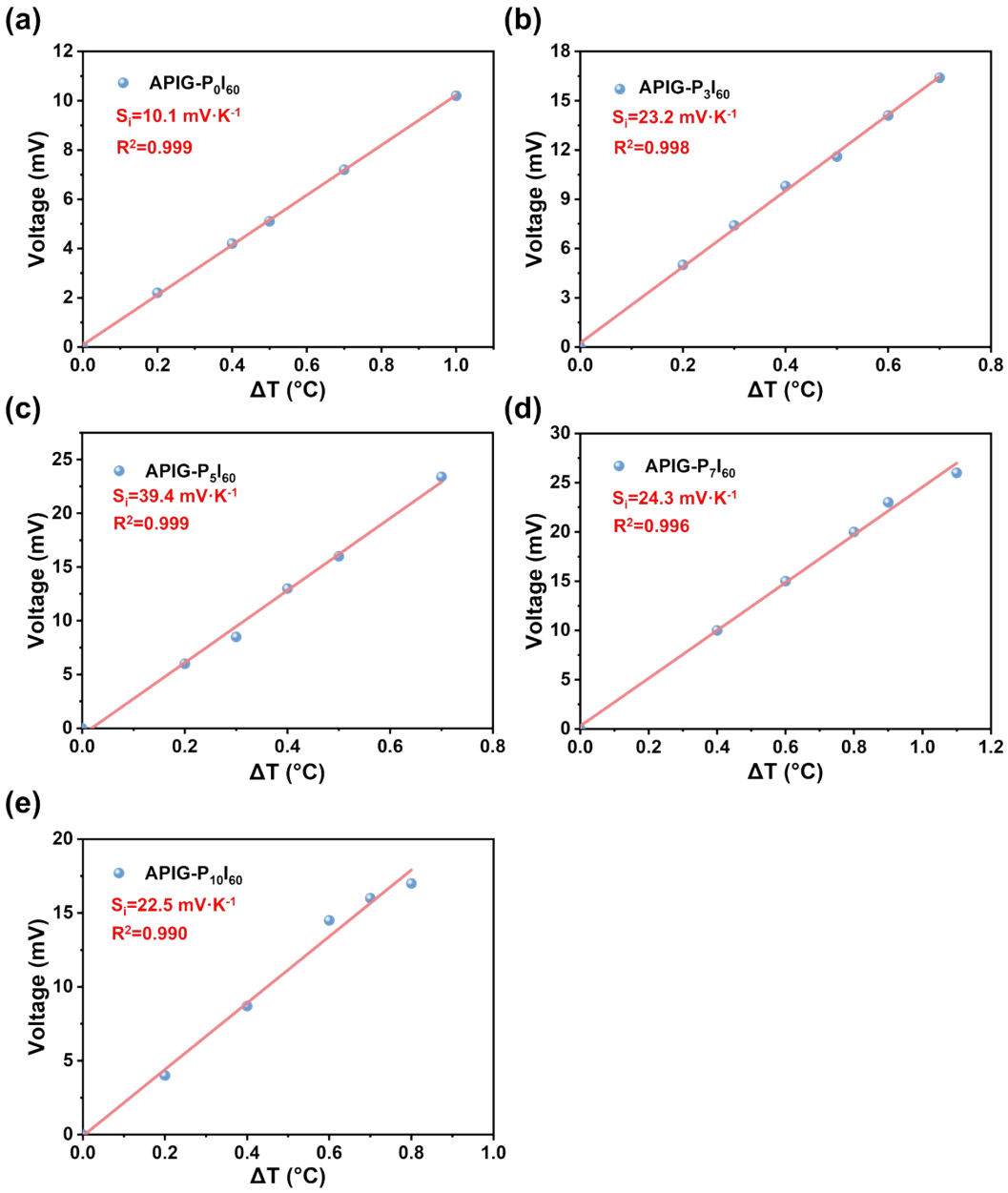

Figure S19. Determination of the Seebeck coefficient of APIG with different POSS-8SH loading concentration of a) APIG-P_0I_{60}, b) APIG-P_3I_{60}, c) APIG-P_5I_{60}, d) APIG-P_7I_{60}, and e) APIG-$P_{10}I_{60}$ by the linear fitting of the open circuit voltage versus temperature gradient.

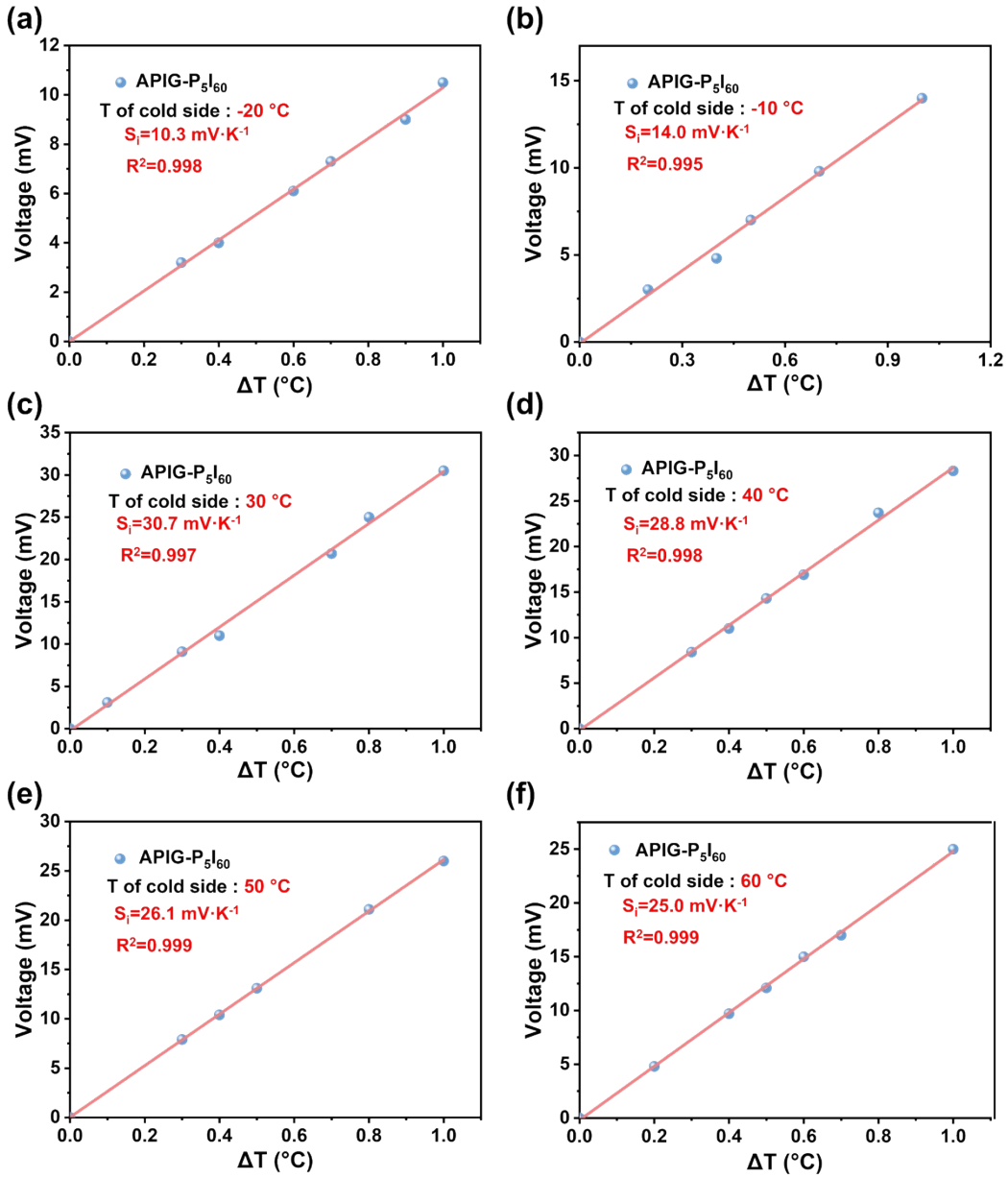

Figure S20. Determination of the Seebeck coefficient of APIG-P_5I_{60} at -20 ℃, -10 ℃, 30 ℃, 40 ℃, 50 ℃ and 60 ℃ by the linear fitting of the open circuit voltage versus temperature gradient.

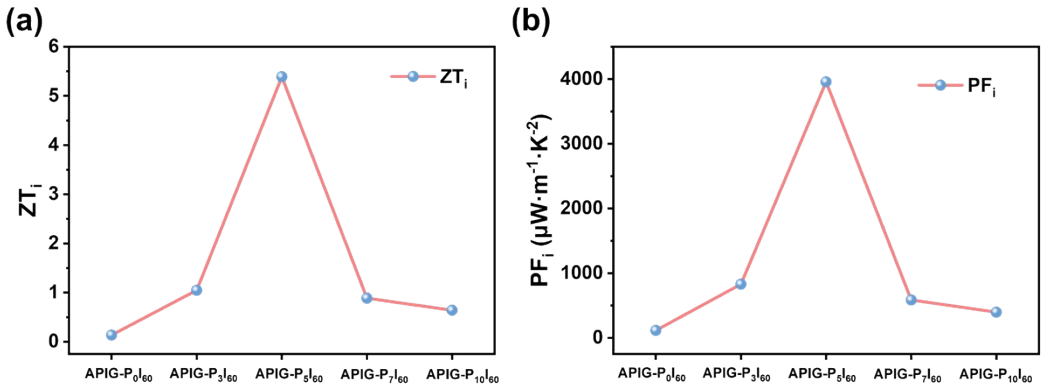

Figure S21. Effect of POSS-8SH contents on the a) ZT_i and b) PF_i of APIG-I_{60}, the ZT_i value exhibits an inverted V-shaped variation with the content of POSS-8SH, and the maximum ZT_i value of 5.39 was achieved for the APIG-P_5I_{60}. The PF_i value also exhibits the same trend, and the maximum PF_i value of APIG-P_5I_{60} reaches 3958.5 $\mu W \cdot m^{-1} \cdot K^{-2}$.

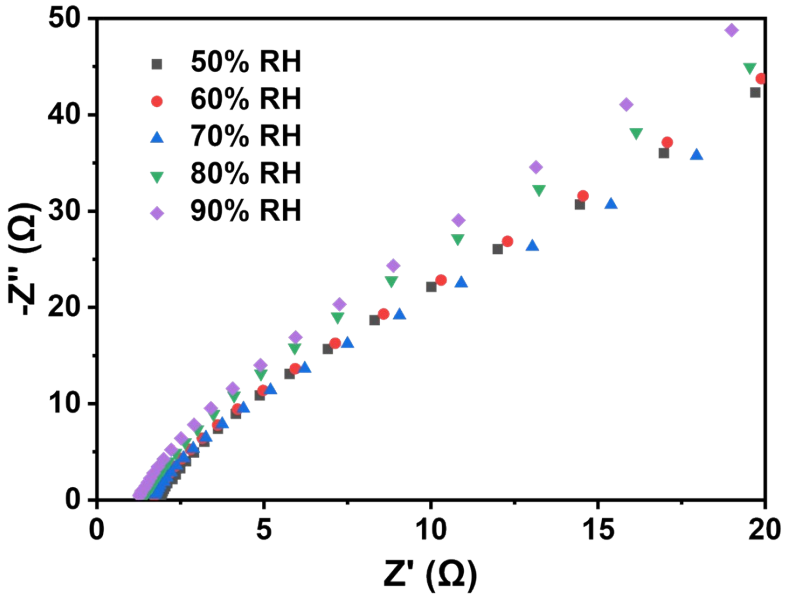

Figure S22. Nyquist plot of APIG-P_5I_{60} under 50%-90% relative humidity.

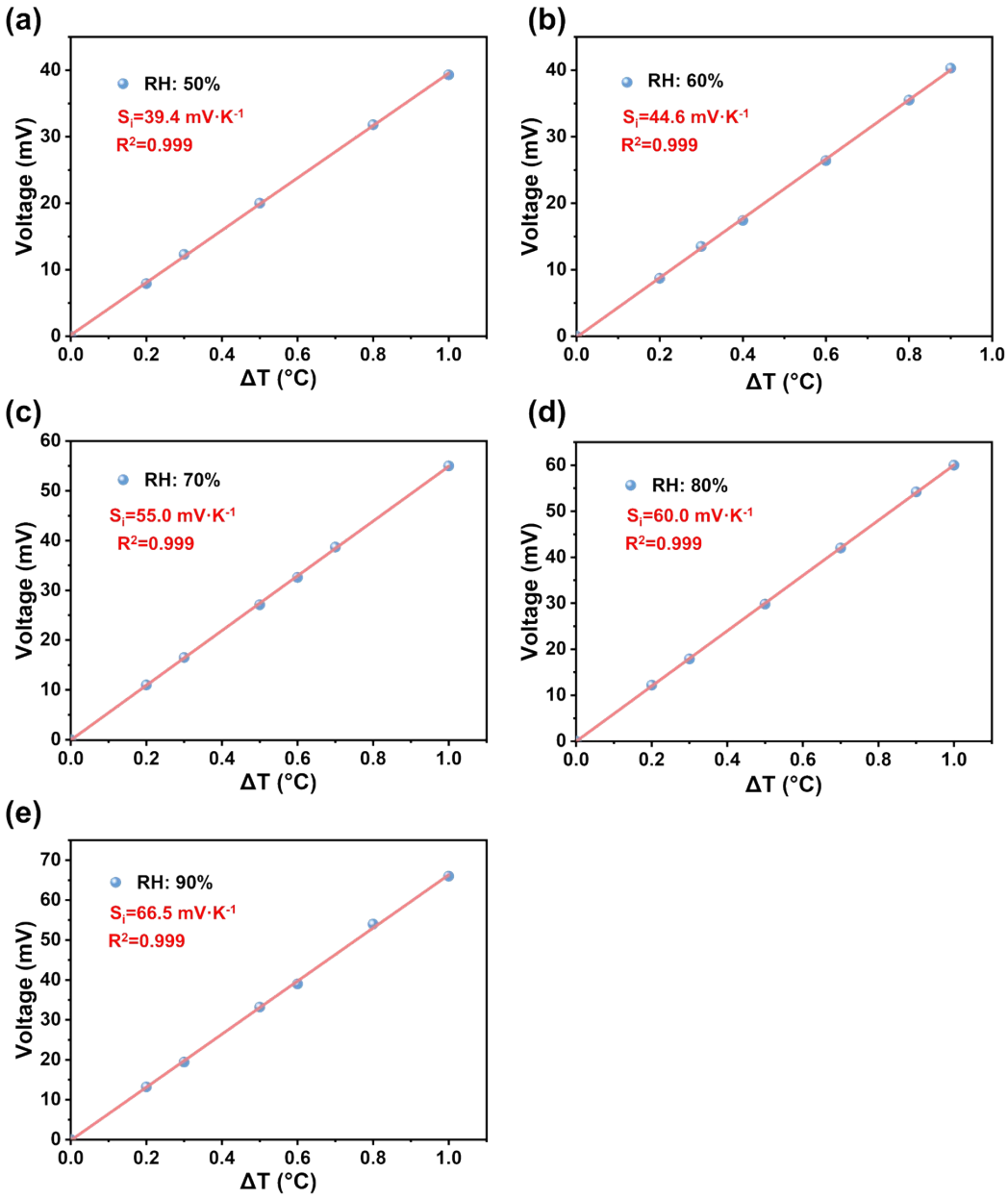

Figure S23. Determination of the Seebeck coefficient of APIG-P_5I_{60} by the linear fitting of the open circuit voltage versus temperature gradient under 50%-90% relative humidity.

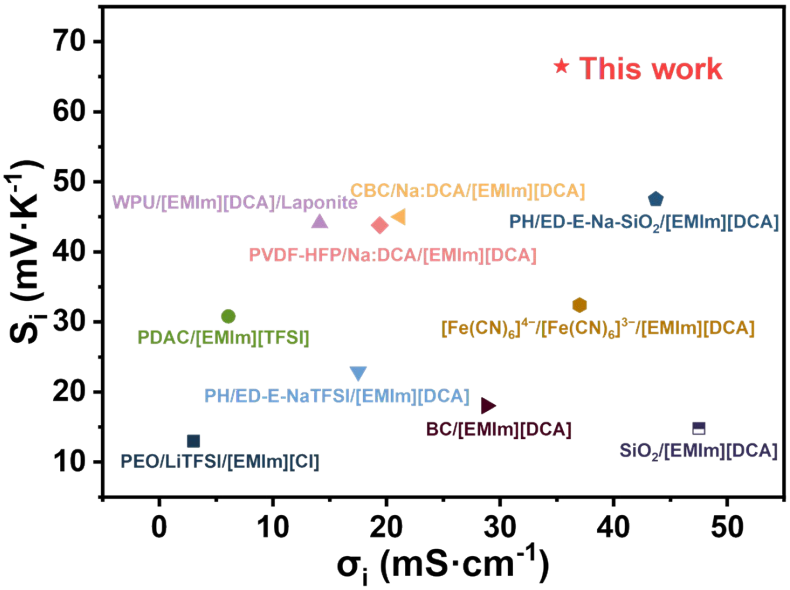

Figure S24. Comparison of the ionic Seebeck coefficient and ionic conductivity of this work with the representative ionogels in literatures.

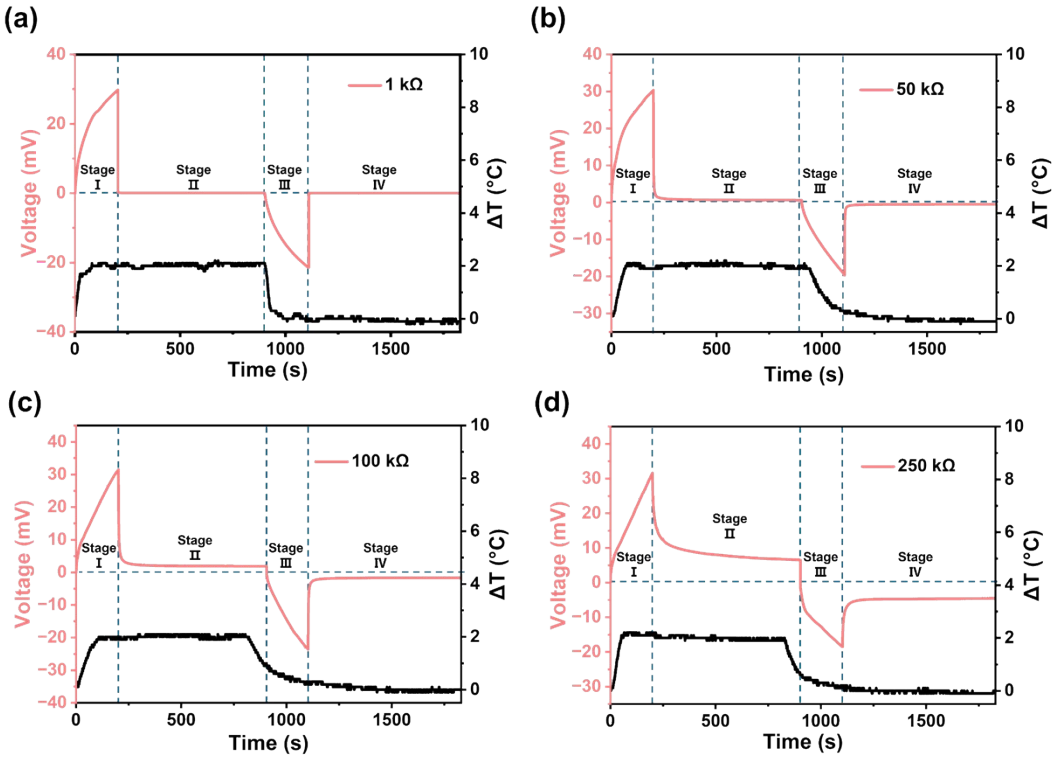

Figure S25. Voltage profiles of the APIG-P_5I_{60}-based ionic thermoelectric supercapacitor connected to an external load under a temperature gradient of 2 ℃ with the resistances of a) 1 kΩ, b) 50 kΩ, c) 100 kΩ, and d) 250 kΩ.

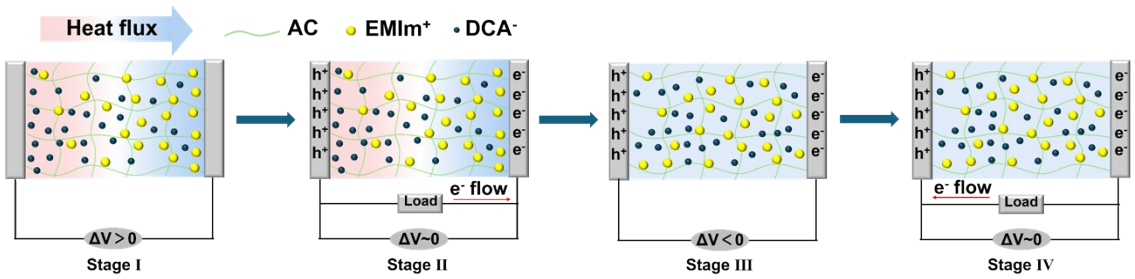

Figure S26. Schematic illustration of the working mechanism and four stages of an ITEC cycle.

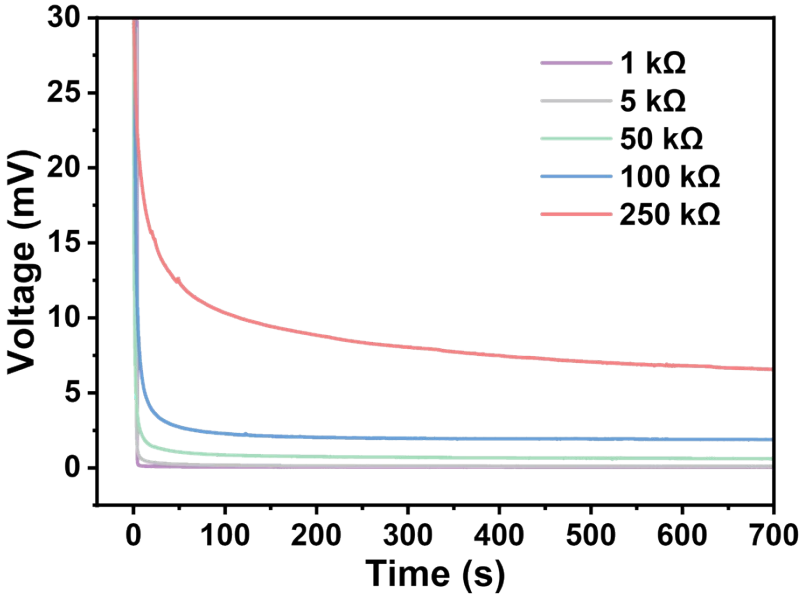

Figure S27. Discharging curves of ITEC connected with different external loading resistances during stage II.

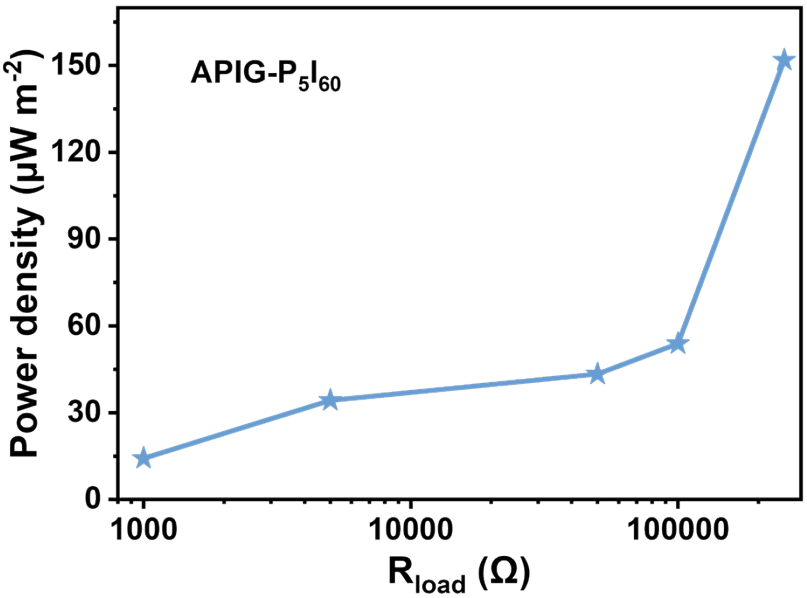

Figure S28. Average power density supplied by the ITECs with APIG-P_5I_{60} during stages II and IV on the resistance of the external load, the power density increases as the impedance rises, and the APIG-P_5I_{60}-based ITEC delivered a compelling average power density of 151.89 $\mu W \cdot m^{-2}$.

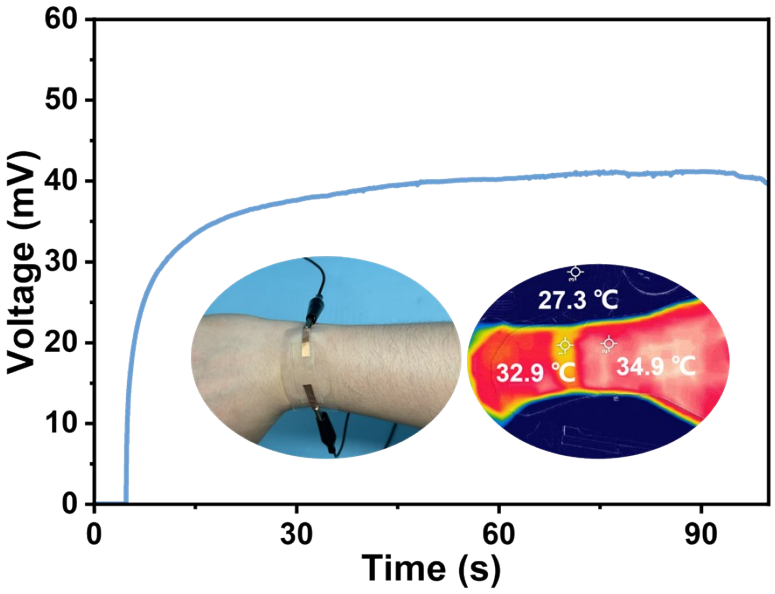

Figure S29. Temperature gradient and thermovoltage generated when wearing the APIG-P_5I_{60}.

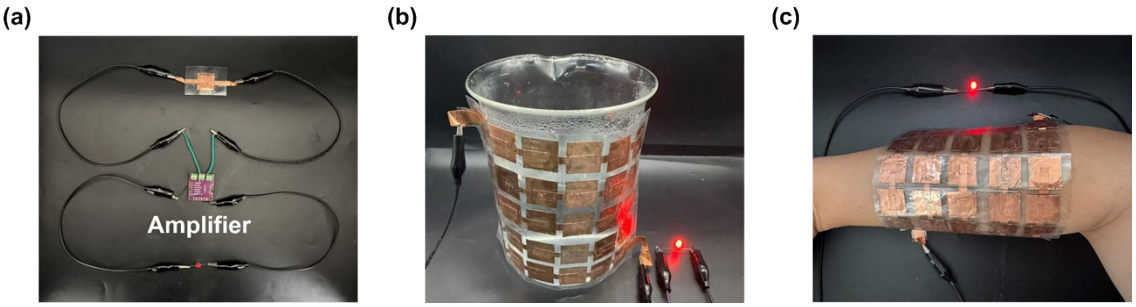

Figure S30. a) Photograph of the circuit connection for lighting up a small light bulb via the APIG-P_5I_{60} thermoelectric device and amplifier. b) Demonstration of an integrated array lighting up a small LED. c) Proof-of-concept image of APIG-P_5I_{60} integrated array worn on the human arm to light LEDs.

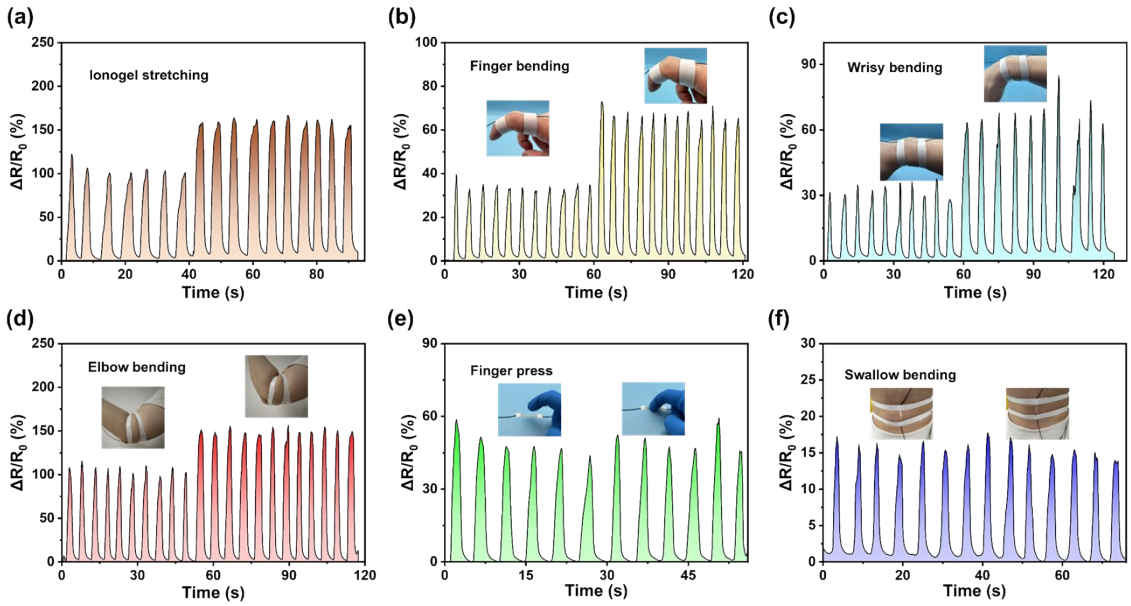

Figure S31. a-f) Sensing detection of human movement by the APIG-P_5I_{60} device. Relative resistance changes for a) ionogel stretching, b) finger bending, c) wrist bending strain, d) elbow being bent, e) finger pressing, f) during swallowing.

References

S1. Q. Li and H. Ardebili, J. Power Sources, 2016, **303**, 17-21.
S2. L. Kong, F. Zhao, J. Li, F. Meng and W. Xu, Adv. Sci., 2025, **12**, e09400.
S3. H. Cheng, X. He, Z. Fan and J. Ouyang, Adv. Energy Mater., 2019, **9**, 1901085.
S4. A. K. Verma, A. S. Thorat and J. K. Shah, J. Ionic Liq., 2024, **4**, 100089.
S5. Y. Cao, Y. Wang, H. Li and W. Chen, Coatings, 2023, **13**, 1799.
S6. C. Qiu, Y. Wang, Y. Li, X. Sun, G. Zhuang, Z. Yao, S. Deng and J. Wang, Green Energy Environ., 2020, **5**, 322-332.